Effects of Flow Unsteadiness on the Transport of Bimodal Bed Material

Gokcen BOMBAR[1]
Aysegul OZGENC AKSOY[2*]
Mehmet Sukru GUNEY[3]

ABSTRACT

The grain size distribution of the bed load was experimentally investigated under unsteady flow conditions with bimodal mixture of sand and gravel in a laboratory flume. Five various triangular hydrographs were generated. A clockwise behavior for the total bed load versus shear velocity was observed meaning that the bed load during rising limb was higher than that of falling limb. It was found that the percent finer at the plateau of bimodal sediment size distribution curve had higher values during the initial and final phases compared to those obtained during the peak time. At all plateaus, the percent finer values related to the hydrograph peak discharge were in the same order of magnitude with that of the bed material. The sand content of the transported bed material initially decreased, then maintained a constant value during a certain time interval and finally returned to its original value. The sand percent of the bed load decreased in the falling limb showing a counterclockwise loop and within the limits of the experimental campaign, the duration of the hydrograph did not affect the results considerably. Greater peak flow rate of the hydrograph resulted in greater hysteresis. The bimodality index was calculated for all transported sediment samples and it was revealed that its initial and final values were less than that of the bed material but it was approximately the same elsewhere. The 5% finer sediment amount was nearly equal during rising and falling limbs. It was revealed that D_{50} value of the bed load decreased in the rising limb showing a clockwise loop. The hysteresis was not considerably changed according to the hydrograph characteristics. The clockwise type hysteresis was also observed for the size group of D_{95}. The lag increased as the peak flow rate increased. A strong relation was found between the dimensionless total bed load W_t^* and the total work index W_k as well as W_k and the ratio W_R/W_F. The correlations between the dimensionless total bed load and the

1 İzmir Katip Çelebi University, Department of Civil Engineering, Izmir, Türkiye
  gokcen.bombar@ikcu.edu.tr - https://orcid.org/0000-0002-8156-6908

2 Dokuz Eylül University, Department of Civil Engineering, Izmir, Türkiye
  aysegul.ozgenc@deu.edu.tr - https://orcid.org/0000-0001-8779-5499

3 İzmir Ekonomi University, Department of Civil Engineering, Izmir, Türkiye
  sukru.guney@ieu.edu.tr - https://orcid.org/0000-0003-1441-4784

* Corresponding author

unsteadiness parameters P, and P_{mod} were very weak, whereas a quite high value of determination coefficient was obtained with the unsteadiness parameter P_{gt}, implying an appreciable interdependence.

Keywords: Unsteady flow, mixed gravel and sand, bimodal sediment, bed load, unsteadiness parameter, hysteresis.

1. INTRODUCTION

The wide range of grain sizes found in most rivers, especially rivers with gravel bed, complicates the problem of the prediction of bedload transport rate. The grain size influences sediment transport and when the sediment bed is a mixture of different grain sizes, the relative size effects become important (Wilcock, 1993, 2001; Wilcock et al, 2001, Wilcock and Kenworthy, 2002). This effect is very sensitive to the composition of the mixture (Houssais and Lajeunesse 2012).

A gravel-bed river has bed material whose characteristic size is in the range of gravel or coarser material. The grain size distributions of most streams show bimodal characteristic. Their particle size distributions are described by a bimodal distribution, i.e. a distribution with two distinct peaks in the frequency distribution, one in the finer and other in the coarser fraction (Sambrook Smith et al. 1996, Müller et al, 2008). Such streams exhibit both sand and gravel modes.

In this study significant quantities of both gravel and sand are present. Studies related to bimodal sediments have been focused on their origin, spatial extent and, more recently, the processes occurring within them. Bimodality may occur readily and be spatially widespread. Bimodal beds may represent a distinct threshold between gravel- and sand-bed states (Sambrook Smith 1996). Since the rivers are often characterized as strongly bimodal (Parker, 2008) it is appropriate to further study the transport of bimodal sediments in order to understand the surface sorting, downstream fining and morphology and ecology of streams. As an example, Tian and Wang (2009) explored the effect of bimodal sediment distribution and its relation with the river ecology in the Dadu river basin by field investigations. The transport and sorting are particularly important in unsteady flows.

Various studies have examined bedload transport under unsteady flow conditions, particularly in the case of uniform sediment. For example, Reid et al. (1985) observed point-bars and associated scour pools at meanders during floods, with no well-developed bed forms at straight reaches. Kuhnle (1992) found that bedload transport rates were higher during the rising limb at high flows, while transport rates were higher during the recession limb at low flows. Qu (2002) observed a time lag between friction velocity and bedload transport, with flow unsteadiness affecting the lag. Lee et al. (2004) investigated bedload transport in a recirculating tilting flume and found that the total yield during the falling period was higher than during the rising period with a counterclockwise hysteresis.

Other studies have focused on mixed sediment beds under unsteady flow conditions. Saadi (2008) examined the stability of mixed bimodal grain sediment beds exposed to different durations of uniform antecedent flow hydrographs and found that longer exposure time increased bed stability. Bombar et al. (2011) investigated the dynamic behavior of sediment transport and proposed an unsteadiness parameter based on net acceleration. Güney et al. (2013) studied the effect of coarse surface development on the bimodal bed-load transport

under unsteady flow conditions. Mao (2012) analyzed sediment transport dynamics during different hydrographs and found that transport during the falling limb was lower than during the rising limb. Wang et al. (2013) studied the transport of bedload mixtures with different grain size distributions and found that coarser fractions reached peak transport rate during the rising limb, while finer fractions reached peak transport rate during the falling limb. Wang et al. (2014) revealed that coarser fractions reached their peak transport rate during the rising limb, while finer fractions typically reached their peak transport rate during the falling limb, which was attributed, at least in part, to the role of sub-threshold, antecedent base flow conditions in restructuring the bed surface grading. Later Wang et al. (2015) indicated that the unimodal sediment bed was inherently more stable than the bimodal bed due to the increased abundance of medium-sized gravels present in the unimodal sediment grade.

The effect of sediment composition on sediment transport in unsteady flow conditions has also been studied. Waters and Curran (2015) found that bedload yields were larger and more variable for sand/silt mixtures compared to sand/gravel mixtures. Tabarestani and Zarrati (2015) suggested that methods based on steady flow conditions underestimate sediment transport rates in unsteady flows and recommended further research on the effect of non-uniform stream bed composition. Gunsolos and Binns (2017) reviewed studies on sediment transport in unsteady flow conditions and emphasized the importance of sediment transport mode and composition in determining hysteresis patterns. Mrokowska and Rowinski (2019) summarized the impact of flow properties and sediment attributes on bedload transport and highlighted the need to quantify the effect of kinematic sieving in multi-modal sediment during flood events. Yarnell et al. (2016) tracked the movement of tracer grains in a gravel-bedded stream and found that larger storms moved a greater percentage of tracers downstream, with no significant variation in grain size distribution between storms. Li et al. (2018) investigated sediment transport under degrading channels and found that sand promoted the transport of gravel, while gravel hindered the transport of sand, with the effect being more pronounced at lower discharges and weakened by flow unsteadiness. Mao (2018) simulated hydrographs as a sequence of events and explored the effect of different antecedent conditions on sediment transport. Their results showed a low-magnitude antecedent event did not affect the rate of sediment transported by a subsequent high-magnitude flood, but a high-magnitude antecedent event reduced the sediment transported by a subsequent long-duration/low-magnitude event. Perret et al. (2018) studied the effect of multimodal sediment composition and the infiltration of fine sediment into the gravel matrix. Khosravi et al. (2019) evaluated the transport of uniform and graded sediment mixtures and found that the transport rate differed for fine and coarse fractions, with coarser fractions exhibiting higher mobility during the rising limb and finer fractions during the falling limb. Duan et al. (2020) compared bedload transport under steady and unsteady flow conditions and found that sediment particles were easier to transport under unsteady flow and moved greater distances. Plumb et al. (2020) observed hysteresis loops in both total and fractional transport, with longer duration hydrographs exhibiting more pronounced loops. Wang et al. (2021a, b) generated symmetrical hydrograph flows over a graded sediment bed and found that coarse size fractions exhibited clockwise hysteresis, while fine transported material showed counterclockwise hysteresis.

The hydrographs can be characterized by various parameters. The total flow work index, W_k is expressed as follows (Lee et al, 2004):

$$W_k = \frac{u_{*0}^2 V_{ol}}{g h_b^3 b}$$
(1)

where u_{*0} is the shear velocity of the base flow at the upstream end, V_{ol} is the total volume of water under the hydrograph (excluding the base flow), g is the gravitational acceleration, h_b is the initial flow depth (base flow) and b is the channel width.

The dimensionless total bed load W_t^* is expressed as (Bombar et al, 2011, Gumgum and Guney, 2021, Przyborowski et al, 2022):

$$W_t^* = \frac{W_t}{\rho_s b D_{50}^2}$$
(2)

where W_t is total bed load, and ρ_s is density of the sediment. W_t^* is used also in scour studies under live bed conditions.

The unsteadiness character of the flow was investigated through various dimensionless parameters. Lee et al. (2004) proposed the following unsteady flow parameter P

$$P = \frac{h_p - h_b}{t_d u_{*0}}$$
(3)

where h_p and t_d denote the flow depth corresponding to the peak flowrate and the total duration of the hydrograph, respectively.

The unsteady flow parameter suggested by De Sutter et al. (2001) is:

$$P_{mod} = \frac{h_p - h_b}{t_r\left[(u_b + u_p)/2\right]} \frac{u_{*p}^2 - u_{*cr}^2}{u_{*cr}^2}$$
(4)

where u_{*p} is the shear velocity at peak flow and u_{*cr} is the critical shear velocity, u_b, u_p denote the cross-sectional mean velocity corresponding to base and peak flow-rates, and t_r is the rising duration of the hydrograph.

The unsteady flow parameter P_{gt} introduced by Bombar et al (2011) is expressed as follows:

$$P_{gt} = \left| S_0 - \left[\frac{u_p - u_b}{g\, t_r} \right] \right| \qquad (5)$$

at which S_0 is the channel bottom slope.

In this study, a set of triangular shaped hydrographs having rising and falling durations of 120 seconds to 300 seconds, from the steady state value of 8.6 l/s to the peak value of 50 l/s and 92 l/s were generated in order to investigate the effects of the flow unsteadiness on the transport of bimodal bed materials.

2. EXPERIMENTAL SET-UP, INSTRUMENTATION AND THE SEDIMENT CHARACTERISTICS

2.1. Experimental Set-Up

Experimental studies were carried out on an experimental system involving a rectangular flume 80 cm wide and 18.6 m long. The bottom slope of the flume was 0.006 and it its transparent sides made from plexiglas were 75 cm high. The bed was fixed with small concrete blocks at the first 3 m of the flume giving a total mobile bed length of 15.6 m. The sediment layer thickness was 7 cm along the flume. The sketch of the experimental set-up is given in Figure 1.
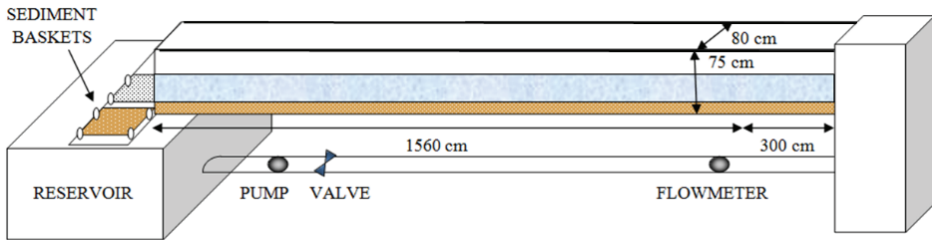

Figure 1 - Scheme of the experimental set-up.

The pump with 100 l/s flow rate capacity was connected to the speed control unit allowing the generation of various shaped hydrographs.

The bed was composed of coarse sand and fine gravel. Before the experiments, the bed was mixed to achieve homogeneity through the vertical and stream-wise directions. The flow rate at the beginning was slowly increased to the base discharge value in order not to disturb the sediments. The experiments were conducted without sediment feeding. The transported bed load was collected in the sediment baskets located at the downstream part of the flume. The grain size distribution was obtained by means of the sieve analysis performed after the collected sediment became dry.

2.2. Instrumentation

The OPTIFLUX 1000 electromagnetic flow meter (manufactured by Krohne) was mounted on the pipe before the entrance of the channel in order to measure the flow rates as Q_{FM}. The ULS– 40D, ultrasonic laboratory water level measuring system was used to measure the water levels in the flume. The IMP+ level monitoring system (Pulsar Process Measurement Limited) was also used to register water depths. The flow depth time series was obtained at x=5 m, 8 m, 11 m, 13.4 m, 15 m and 17 m The velocities were measured by using Ultrasonic Velocity Profiler (UVP) (manufactured by Met-Flow SA) which was located at the entrance of the flume as given in Figure 2. The UVP transducer was placed at the entrance of the flume, looking upwards with an angle of 16 degrees. This configuration helped to determine the flow depths specific to the location that the velocities were measured. The electrolysis was used for the generation of the hydrogen bubbles as seeding particles for the velocity measurements.
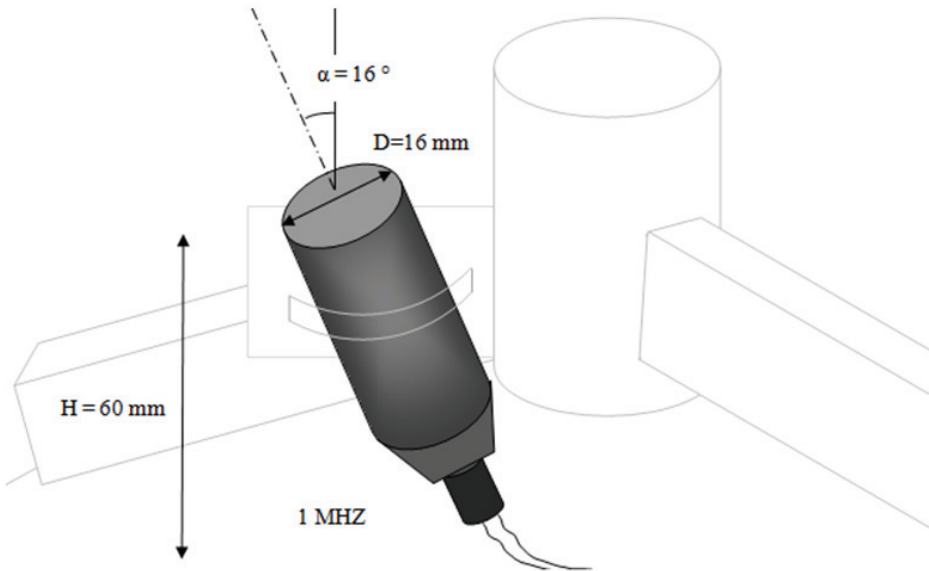

Figure 2 - Ultrasonic Velocity Profile (UVP) transducer configuration

2.3. Bed Material Characteristics

The bed material used in the flume was composed of bimodal sediment mixture. The grain size distribution of the mixture is given in Figure 3. The characteristics of the sediment mixture are given in Table 1. The sediment sizes are calculated by the method and excel sheets given in Gary Parker's Morphodynamics Web Page (2006a,b). The greater sizes such as D_{95} were chosen in accordance with the maximum sediment sizes given in Melville and Sutherland (1988).
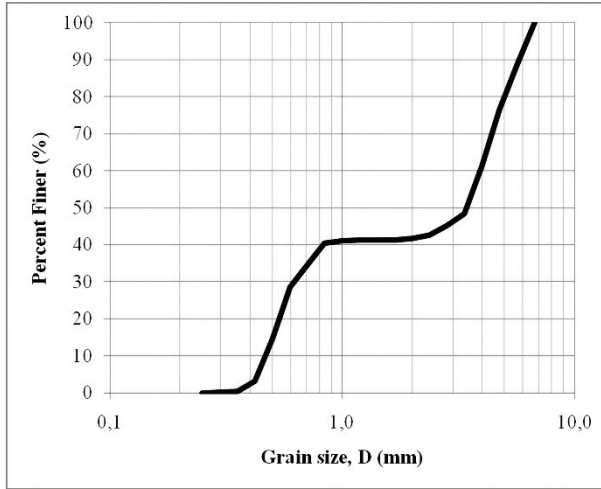
Figure 3 - Grain size distribution of the bed material

Table 1 - Characteristics of the sediment mixture

Parameter	Mixture
Geometric mean size D_g (mm)	1.84
Geometric standard deviation σ_g	2.84
D_5 (mm)	0.45
D_{10} (mm)	0.46
D_{16} (mm)	0.50
D_{30} (mm)	0.61
D_{35} (mm)	0.71
D_{50} (mm)	3.43
D_{60} (mm)	3.88
D_{70} (mm)	4.38
D_{84} (mm)	5.26
D_{86} (mm)	5.41
D_{90} (mm)	5.71
D_{95} (mm)	6.12
D_{96} (mm)	6.20

The sediment less than or greater than 2 mm in size is considered as sand or gravel, respectively. The bimodality index, B* for the particle size distribution in ϕ units

($\phi = -\log_2 D$ where D is particle diameter in mm) was calculated from the following equation proposed by Smith (1997).

$$B^* = \left| \phi_c - \phi_f \right| \left(\frac{P_c}{P_f} \right)$$ (6)

where ϕ_f and ϕ_c are the ϕ-sizes of the fine and coarse mode, respectively and P_f and P_c are the proportions of sediment contained in these two modes. The related values are $\phi_f = -1$, $\phi_c = 2$, $P_f = 14.2$ and $P_c = 15.4$ which give the value of 3.2 for B*. According to Smith et al (1997), bimodality holds when B* > 1.5, implying that the studied sediment is highly bimodal.

Another definition of bimodality index, denoted by B, is given by Wilcock (1993).

$$B = \left(\frac{D_c}{D_f} \right)^{1/2} \Sigma P_m$$ (7)

where D_f and D_c are the grain sizes of the fine and coarse mode, respectively and ΣP_m is the sum of the proportion in mode. The value of B was found to be equal to 2.8 meaning that the sediment is bimodal since the limit value is 1.7.

The incipient motion and bed load calculations were performed by using the median grain size according to the method proposed by Wilcock, (1988) (Güney et al., 2013).

3. ANALYSIS OF RESULTS

3.1. Experimental Results

Experiments were conducted using 5 different triangle shaped input hydrographs. The characteristics of the hydrographs, predefined by a computer software and generated by using the control unit connected to the pump, are given in Table 2 where Q_b, Q_p represent the base and peak flow rates, respectively, calculated by the velocity and flow depth measured by UVP at the entrance. In the table, h_b, h_p represent the base and peak flow depths and u_b, u_p represent the base and peak velocities determined by UVP. The discharge values were measured by means of the flowmeter placed on the the pipe supplying water to the channel. The hydrograph generated at the discharge pipe of the pump was attenuated during its propagation through the flume and lower values of base and peak flow depths were registered in the channel. $h_{b\ x=13.4\ m}$ and $h_{p\ x=13.4\ m}$ denote the base and peak flow depths measured in the channel at x = 13.4 m downstream of the entrance of the flume. The t_r, t_f and t_d, are the rising, falling and total durations of the hydrograph respectively. Fr_{base} and Fr_{peak} refer to the Froude numbers calculated for base and peak flow rates, respectively. The Froude numbers given above were calculated by using these flow depths and corresponding velocity

values obtained by UVP. Froude numbers being smaller than unity indicates the subcritical character of the experimental conditions.

Table 2 - Characteristics of the hydrographs and flow parameters used in this study

Experiment	Exp-1	Exp-2	Exp-3	Exp-4	Exp-5
Q_b (l/s)	8.6	8.6	8.6	8.6	8.6
Q_p (l/s)	66.0	72.4	45.6	69.2	92.4
h_b (m)	0.049	0.049	0.049	0.049	0.049
h_p (m)	0.131	0.133	0.114	0.133	0.156
u_b (m/s)	0.22	0.22	0.22	0.22	0.22
u_p (m/s)	0.63	0.68	0.50	0.65	0.74
$Q_{pipe\,p}$ (l/s)	71.0	71.1	49.3	69.7	91.7
$h_{b\,x=13.4m}$ (mm)	37	37	37	37	37
$h_{p\,x=13.4m}$ (mm)	13	11	9.2	11	4-
t_r (min)	2	3	5	5	5
t_f (min)	2	3	5	5	5
t_d (min)	4	6	10	10	10
Fr_{base}	0.32	0.32	0.32	0.32	0.32
Fr_{peak}	0.56	0.60	0.47	0.57	0.60

Triangle-shaped input hydrographs were generated for a total of seven runs to ensure repeatability and reliability of the results. The mean value of each parameter i.e, g_b, D_5, σ_g etc., was calculated to obtain representative results and are presented in the subsequent figures and tables. For instance, equation (8a) was used to obtain the mean value of g_b out of n runs. To investigate the effect of unsteady flow on the size distribution of the sediment mixture, two selected runs were analyzed by performing a sieve analysis for each collected bed load sample. The scattering index for a given time, SI_t, is calculated by dividing root-mean-square error (RMSE) with mean of the runs for that time interval as in the equation (8b). The mean of SI_t values for the runs with sieve analysis and mean of SI_t values for all experiments were determined as given in equation (8c), where m is the number of bed load samples for a specific experiment and presented in Table 3. For illustrative purposes, the relation between the mean of the bed load obtained by considering all repeated runs and those runs conducted for sieve analysis are depicted in Figure 4 for Exp-1 and Exp-3. Complete set of R^2 values are given in Table 3 as well as the SI values for the parameters D_5, D_{50}, D_{95} and σ_g parameters.

$$\overline{g_b} = \frac{1}{n}\sum_{i=1}^{n} g_{bi} \tag{8a}$$

$$SI_t = \frac{\sqrt{\frac{1}{n}\sum_{i=1}^{n}(g_{bi}-\overline{g_b})^2}}{\overline{g_b}} \tag{8b}$$

$$SI = \frac{1}{m}\sum_{t=1}^{m} SI_t \tag{8c}$$

Table 3 - Statistical analysis of the hydrographs and flow parameters used in this study

	Exp-1	**Exp-2**	**Exp-3**	**Exp-4**	**Exp-5**
SI of g_b all runs	0.42	0.34	0.36	0.46	0.27
SI of g_b with sieve analysis	0.33	0.14	0.26	0.31	0.30
R^2	0.9914	0.9925	0.9930	0.9804	0.9989
SI of D_5	0.02	0.03	0.03	0.03	0.03
SI of D_{50}	0.21	0.08	0.17	0.17	0.17
SI of D_{95}	0.08	0.02	0.09	0.20	0.19
SI of σ_g	0.06	0.02	0.04	0.05	0.06
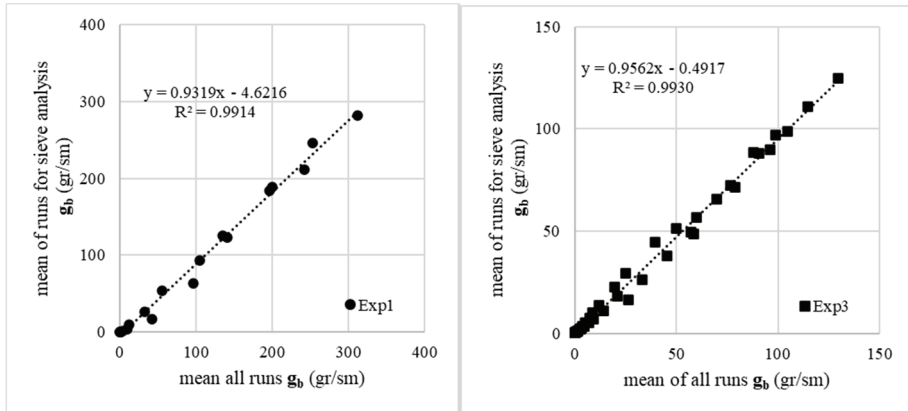
Figure 4 - Relation between the mean of the bed load obtained by considering all repeated runs and those runs conducted for sieve analysis a) Exp-1, b) Exp-3.

The variation of flow rate with respect to time is given in Figure 5. The flow depth variation is given in Figure 6. The cross-sectional mean velocity measured by UVP at the entrance of the flume is given in Figure 7.
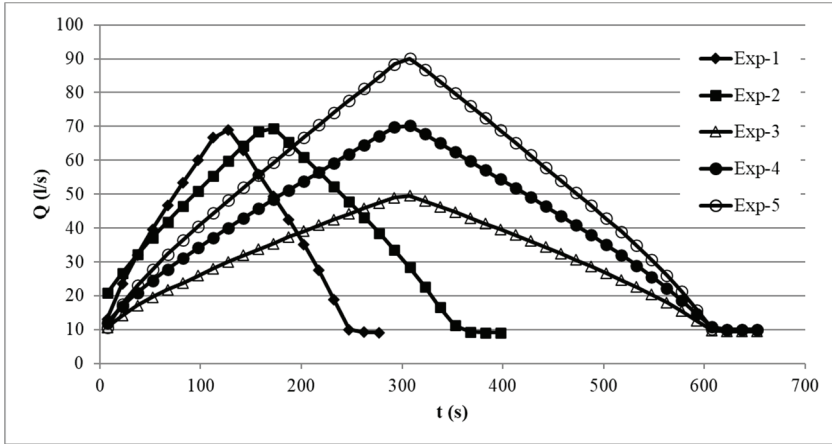
*Figure 5 - Flow rate variations with respect to time*
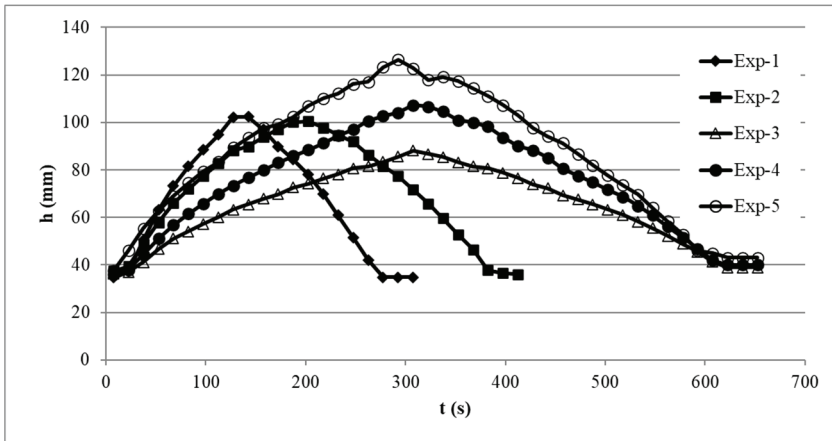
*Figure 6 - Flow depth variations with respect to time*
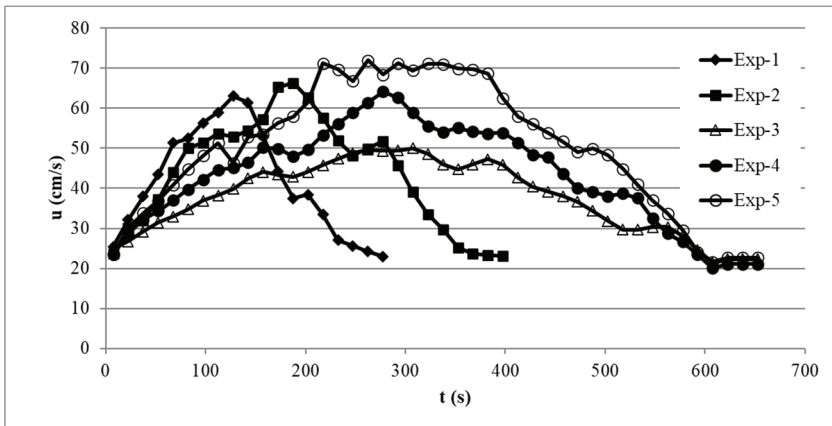
Figure 7 - Cross sectional mean velocity variations with respect to time

The average values of the time variation of the bed load are given in Figure 8. Some bed forms of small magnitude were observed during the experiments.
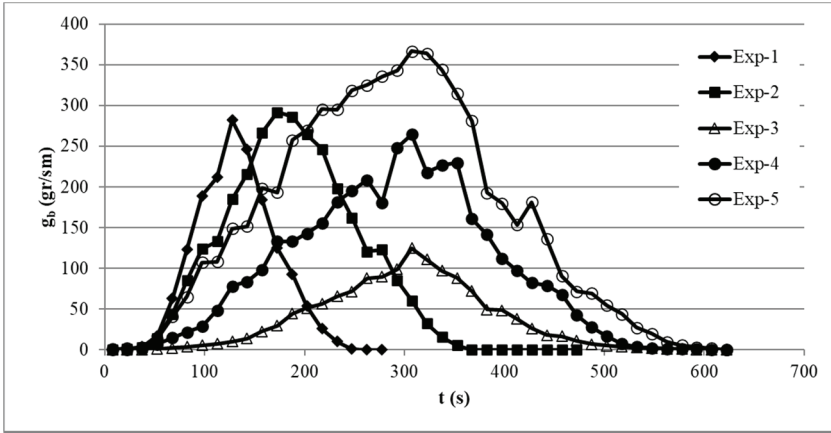

Figure 8 - Bed load variations with respect to time

The shear velocity is calculated by the Equation (9)

$$u_* = \sqrt{g\,R\left(S_0 - \frac{\partial h}{\partial x}\right)} \tag{9}$$

where R is the hydraulic radius, and x is the abscissa.
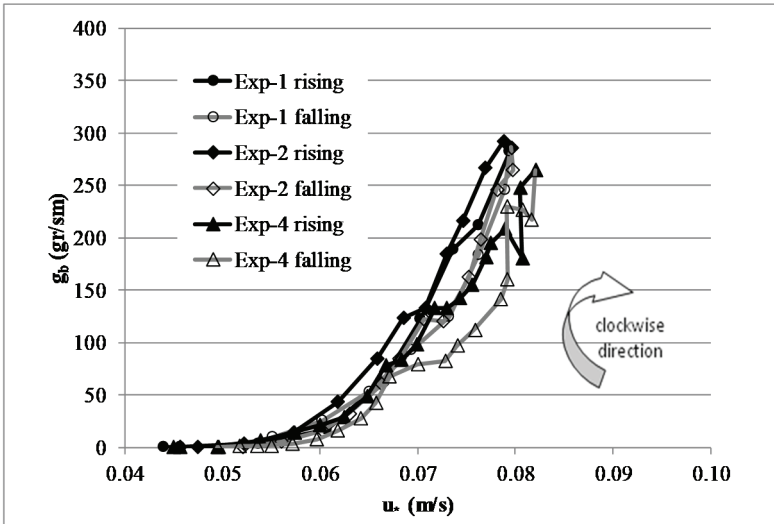

(a)
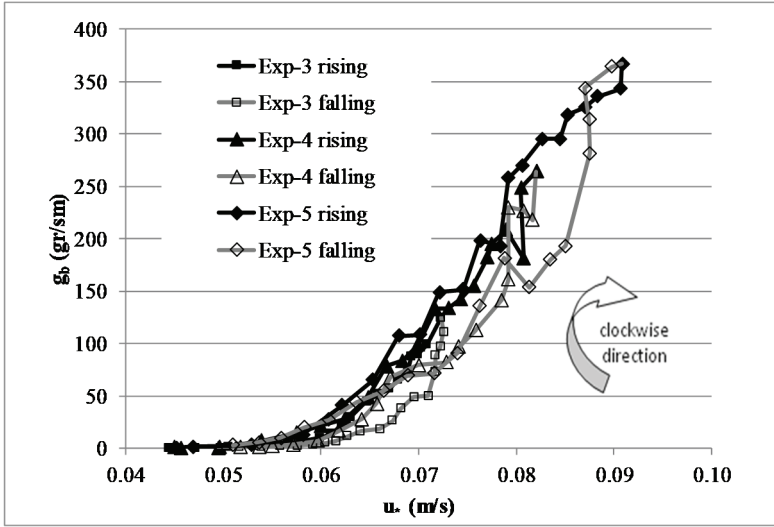
(b)

Figure 9 - Variations of the bed load with respect to the shear velocity for (a) Exp-1, Exp-2 and Exp-4, (b) Exp-3, Exp-4 and Exp-5

The variation of the bed load with respect to the shear velocity is given in Figure 9.a and Figure 9.b. There was a clockwise behavior meaning that the bed load was higher during the rising compared to the falling. This clockwise behavior was also observed by Kuhnle (1992) and Nanson (1974).

3.2. The Grain Size Distribution of Transported Sediment

The sieve analysis was performed for each group of sediments collected in the baskets in order to obtain the variation of the grain size distribution with respect to time. The average values corresponding to the intervals of 1 minute were determined and they are depicted in Figure 10.a to 10.e for the Exp-1 to Exp-5, respectively.

Based on the experimental results, it was observed that the percent finer concerning the plateau had higher value during the initial and final phases compared to those obtained during the peak time. The plateau percentages corresponding to the peak value of the time were close to each other for all hydrographs and they were nearly equal to the initial percentages of the bed material. It was observed that the percent finer value for the highest duration hydrographs (10 minutes) in Exp-3, Exp-4 and Exp-5 were approximately in the same order. The smallest value was found in the case of Exp-1 corresponding to the shortest hydrograph. It was concluded that the location of the plateau was highly influenced by the hydrograph duration.

The time variation of the sand content ratio of the bed load is given in Figure 11. At the beginning of the experiments, the sand content of the transported bed material decreased rapidly from approximately 96 % to 30% – 40% which was the original sand content of the bed material. The sand content remained constant for a while (t_w) and gradually increased at the end of the hydrograph. The values of t_w and t_w / t_r are given in Table 4.

(a)

(b)

(c)
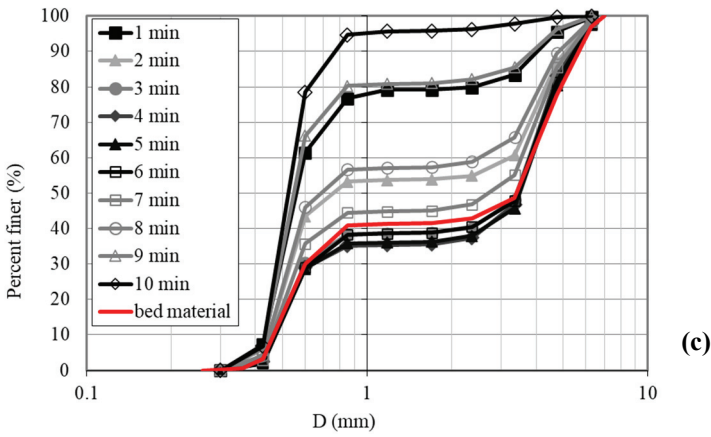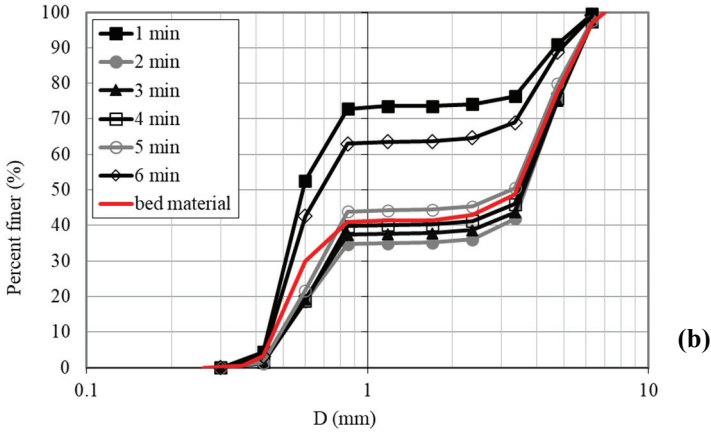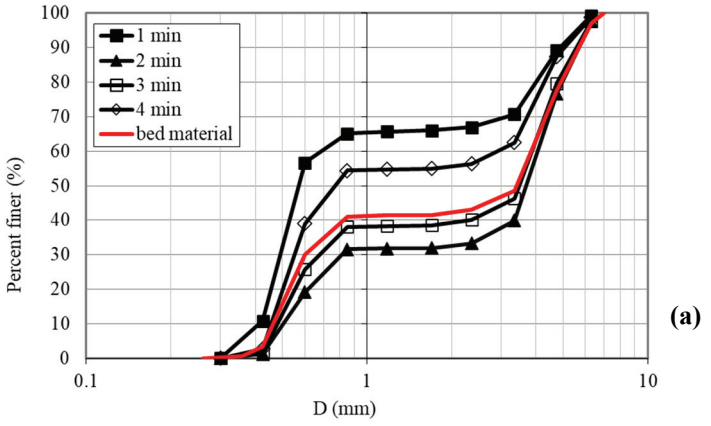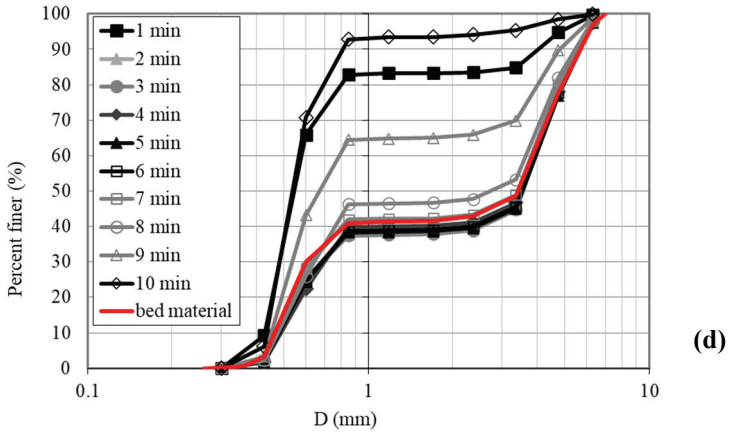
(d)
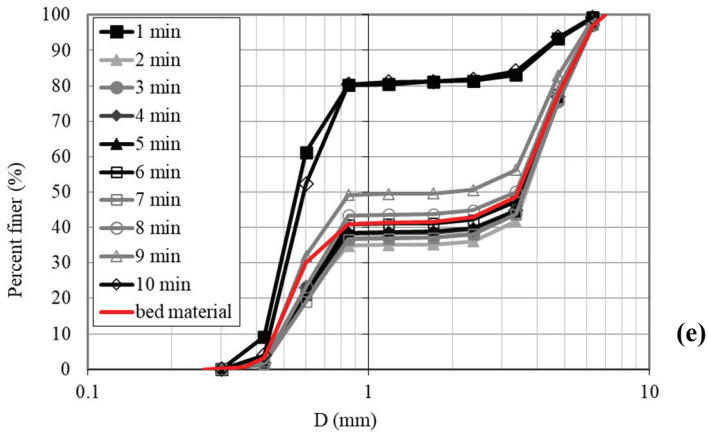
(e)

Figure 10 - Grain size distribution variations with respect to time, (a) Exp-1, (b) Exp-2, (c) Exp-3, (d) Exp-4, (e) Exp-5

During the peak phases, the flow velocity has greater values. When the velocity was low, the flow had not the ability to transport the coarser sediment sizes, and consequently only sand material displaced. On the other hand, when the velocity increased the coarser grains were also included comprising the percentage of the bed load almost of the same percentage existing in the bed material.

The bimodality index B* was calculated and its variation with time is depicted in Figure 12. It was observed that in all experiments the B* increased quickly in the rising limb and then had a nearly constant value slightly greater than unity for bed material. In the falling phase the value of the B* decreased to its original and initial value. The percent contents of sand and gravel for Exp-4 at various times along with percent content of the bed material are given in Figure 13.
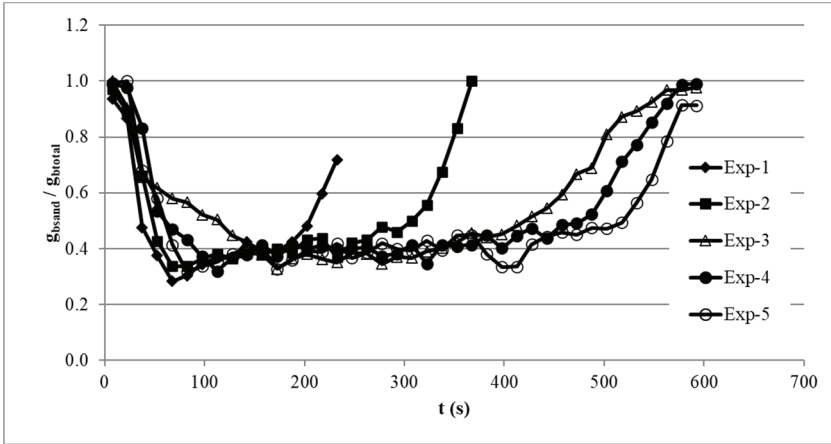
Figure 11 - Time variations of the sand content ratio of the bed load

Table 4 - t_w and t_w / t_r values

Experiment	Exp-1	Exp-2	Exp-3	Exp-4	Exp-5
t_w (s)	100	250	360	410	420
t_w / t_r	0.83	1.33	1.20	1.37	1.40
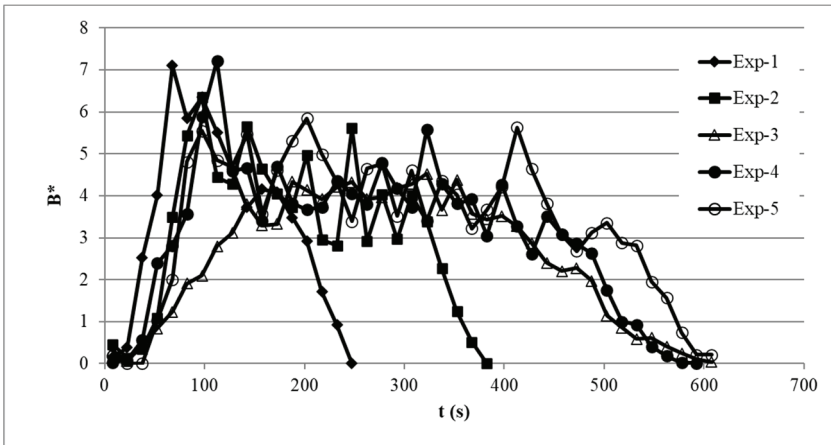
Figure 12 - Variation of Bimodality index B* with time
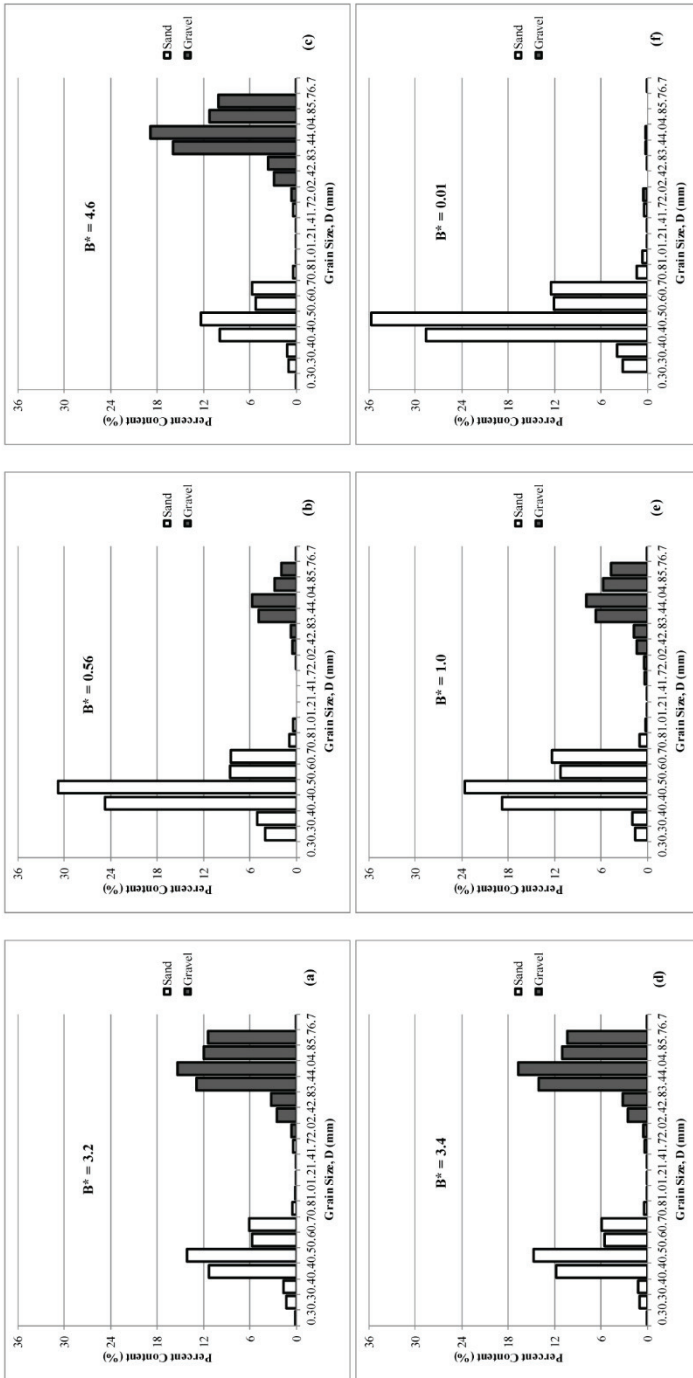
Figure 13 - The percent content of sand and gravel for Exp-4 (a) bed material (b) at t=40 s, (c) at t=130 s, (d) at t=160 s, (e) at t=520 s, (f) at t=580 s

The variations of the percent sand content of the bed load with respect to the shear velocity are given in Figure 14.a and Figure 14.b. It was revealed that the sand percent of the bed load decreased in the falling limb, showing a counterclockwise loop. The duration of the hydrograph was not likely to affect the results considerably. On the other hand, the greater the peak flow rate of the hydrograph, the greater the hysteresis.
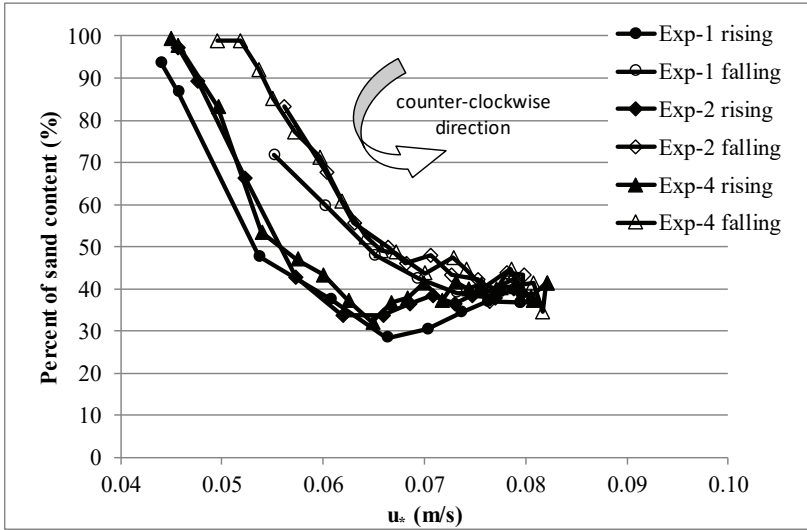

(a)
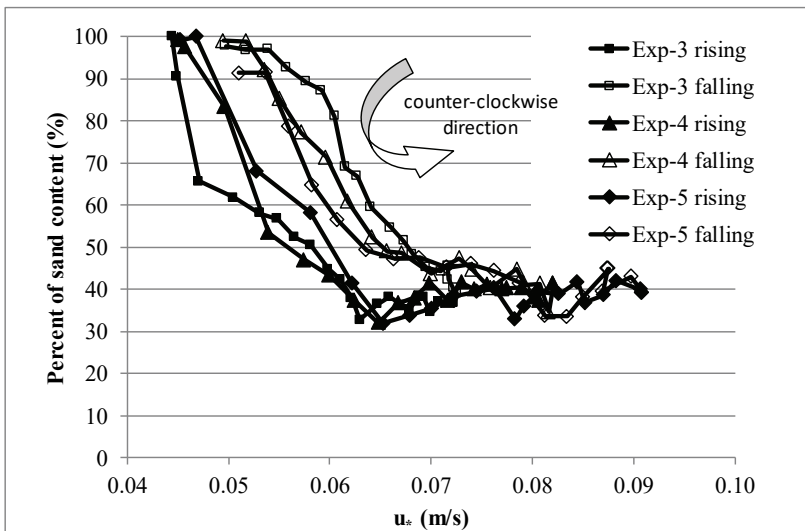
(b)

Figure 14 - Variations of the percent sand content of the bed load with respect to the shear velocity for (a) Exp-1, Exp-2 and Exp-4, (b) Exp-3, Exp-4 and Exp-5

The values of D_5, D_{50} and D_{95} were determined from the cumulative grain size distribution curves of the collected sediments. The variations of D_5 with respect to the shear velocity are given in Figure 15.a and Figure 15.b. The 5% finer sediment amounts were the same for the whole duration of the hydrographs for all experiments.
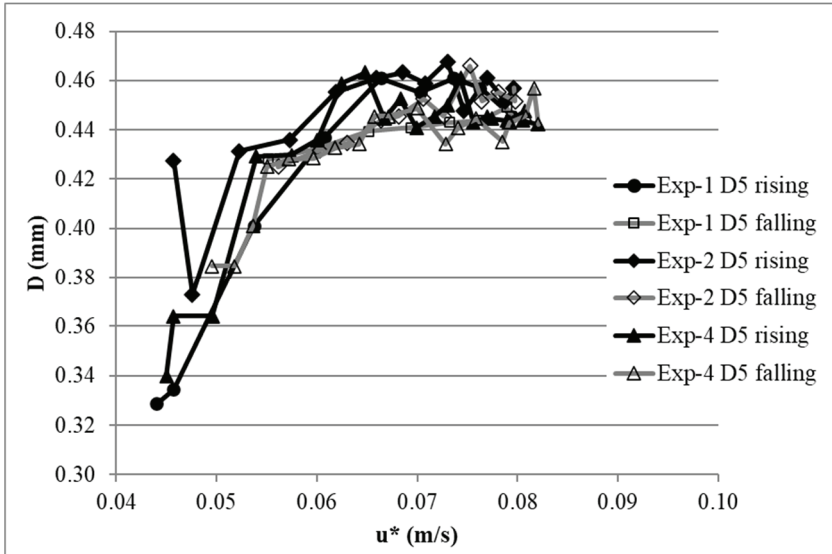

(a)
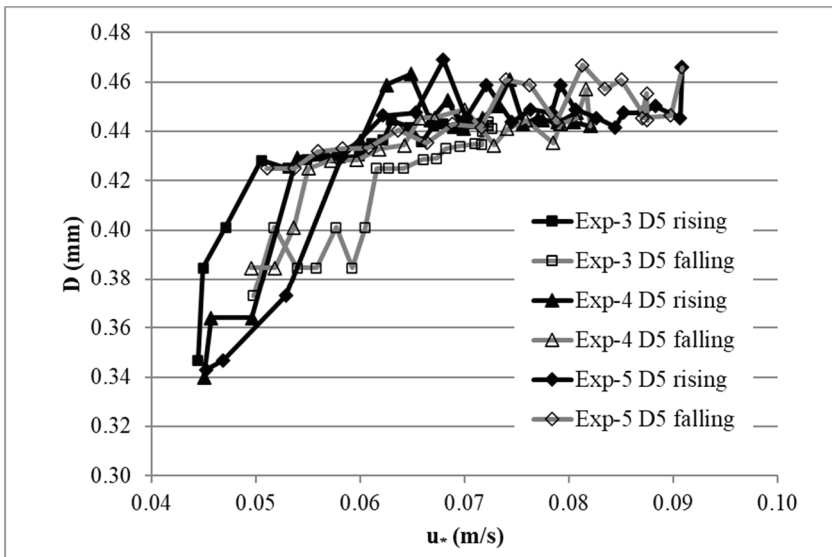
(b)

Figure 15 - Variations of D_5 with respect to the shear velocity, for (a) Exp-1, Exp-2 and Exp-4, (b) Exp-3, Exp-4 and Exp-5

The variations of D_{50} with respect to the shear velocity are given in Figure 16.a and Figure 16.b. It was revealed that D_{50} value of the bed load decreased in the rising limb, showing a clockwise loop. The hysteresis was not considerably changed with respect to hydrograph characteristics.

(a)

(b)
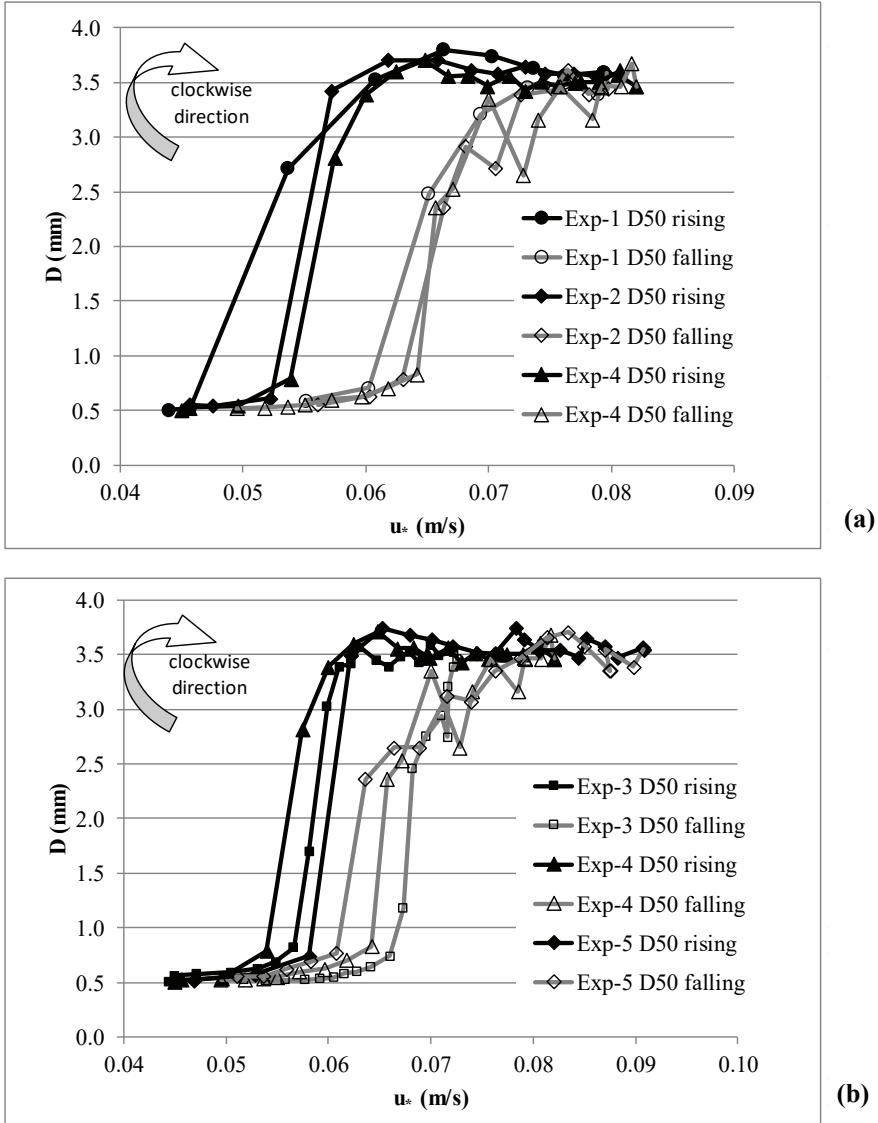
Figure 16 - Variations of D_{50} with respect to the shear velocity, for (a) Exp-3, Exp-4 and Exp-5, (b) Exp-1, Exp-2 and Exp-4

The variations of D_{95} with respect to the shear velocity are given in Figure 17.a and Figure 17.b. The clockwise type of hysteresis was also observed for this size group. The D_{95} in Exp-3, Exp-4 and Exp-5 had an influence on the hysteresis where the lag increased with the increase in the peak flow rate.
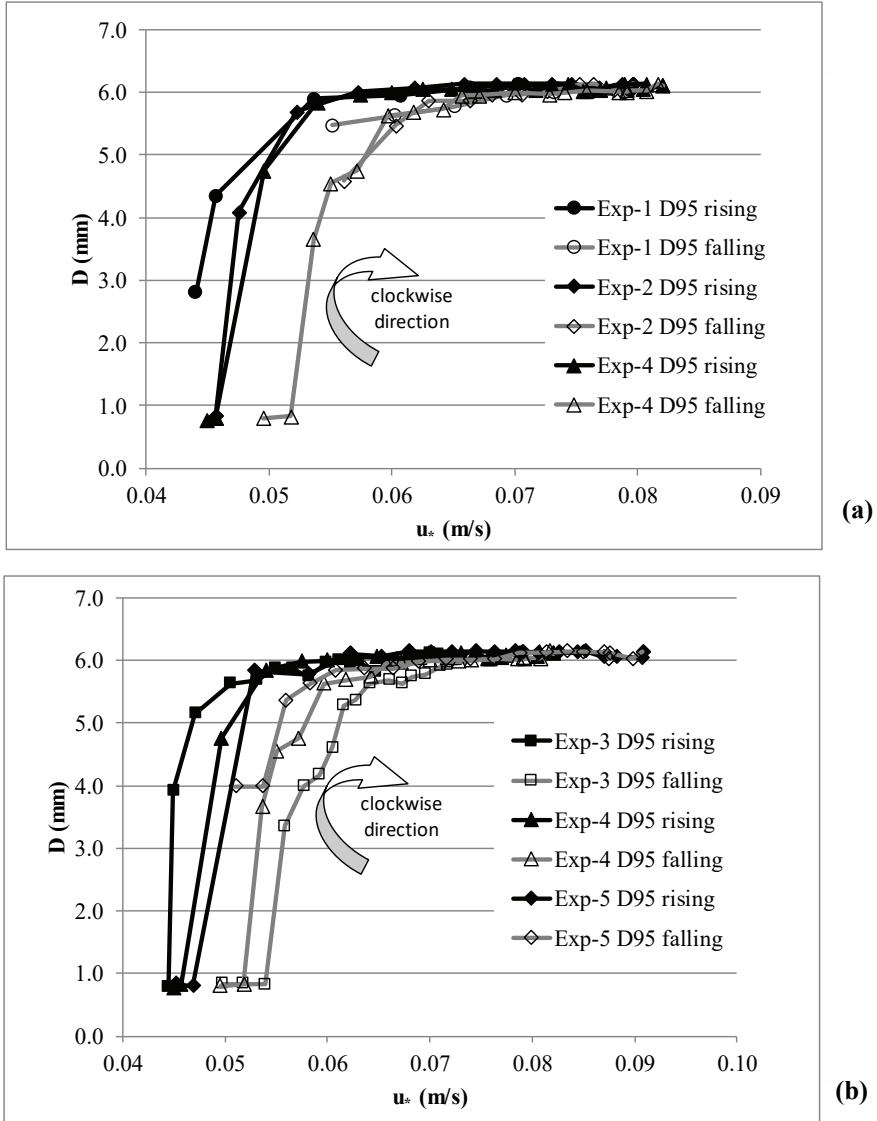

Figure 17 - Variations of D_{95} with respect to the shear velocity, for (a) Exp-3, Exp-4 and Exp-5, (b) Exp-1, Exp-2 and Exp-4

3.3. Total Flow Work Index and Unsteadiness Parameters

The experimental results of the hydrographs and the amount of the bed load collected during the rising and falling limbs of the hydrographs are summarized in Table 5. The total volume was calculated by assuming a basic triangular shape and dimensionless parameters were calculated by using the flow data obtained at the entrance of the flume since both velocity and flow depth values could be measured only at that section.

Table 5 - Experimental results and unsteadiness parameters

| Experiment	Exp-1	Exp-2	Exp-3	Exp-4	Exp-5
Total volume excluding base flow (m^3)	6.9	11.5	11.1	18.2	25.1
W_k	19.2	31.9	30.9	50.5	69.9
W_t (kg)	22.1	37.1	17.6	45.3	77.6
W_t^*	904	1518	721	1853	3371
P	0.0067	0.0046	0.0021	0.0028	0.0035
P_{mod}	0.0026	0.0017	0.0008	0.0011	0.0015
P_{gt}	0.00565	0.00574	0.00590	0.00585	0.00582
u_p^* (m/s)	0.08	0.08	0.07	0.08	0.08

(a)

(b)
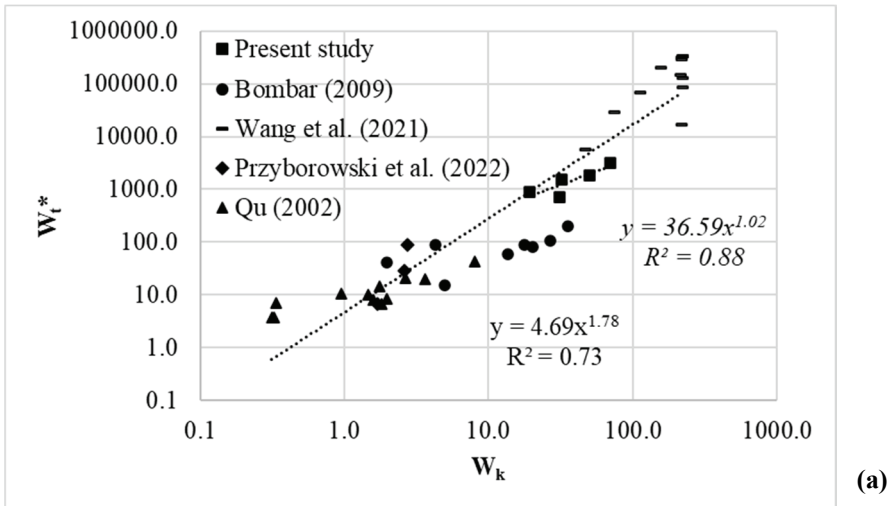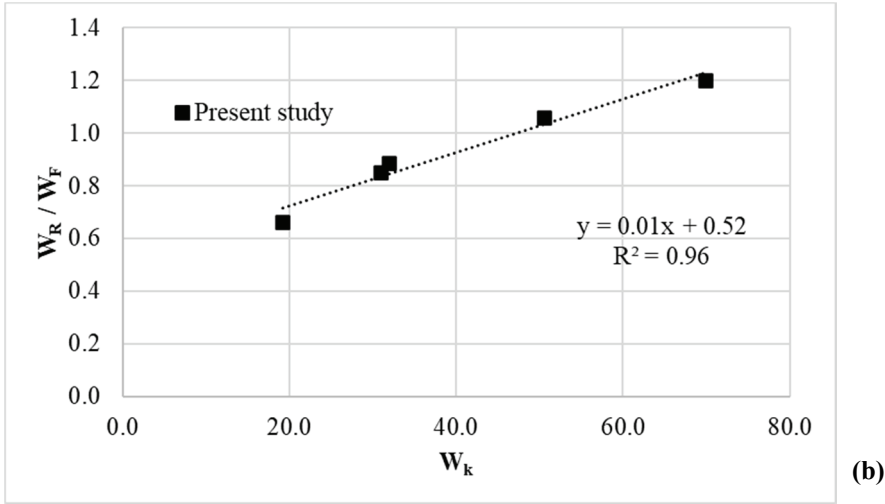
Figure 18 - (a) Variation of W_t* with respect to the total work index W_k, (b) Variation of W_R/W_F with respect to the total work index W_k

The variation of the dimensionless total bed load W_t* with respect to the total work index W_k is presented in Figure 18.a. The data of Bombar (2009), Qu (2002), Wang et al. (2021) and Przyborowski et al. (2022) were also added to the graph. A strong relation (Eq. 10.a) was found between W_t* and W_k with a determination coefficient of $R^2 = 0.88$, when only the data of present study was regarded. When the data mentioned above was also considered the R^2 became 0.73, the SI is calculated as 1.68. and the relation given in equation (10.b) was obtained.

$$W_t* = 36.59 \, W_k^{1.02} \tag{10.a}$$

$$W_t* = 4.69 \, W_k^{1.78} \tag{10.b}$$

By using the equation given above the amount of bed load for a given duration of a hydrograph can be predicted provided that the volume of water that corresponds to the area under the hydrograph is known.

The variation of the dimensionless total bed load W_R/W_F with respect to the total work index W_k is presented in Figure 18.b. The following relation with a determination coefficient of 0.96 and SI as 0.04 were obtained:

$$W_R/W_F = 0.01W_k + 0.52 \tag{11}$$

The values of the unsteadiness parameters P, P_{mod} and P_{gt} calculated from the relevant equalities stated previously are given in Table 4.

The variation of the dimensionless total bed load W_t* versus the unsteadiness parameters P, and P_{mod} were plotted in Figure 19.a and 19.b, respectively together with the data of Bombar

(2009), Qu (2002), Wang et al. (2021) and Przyborowski et al. (2022). The coefficients of determination were very low, particularly for P_{mod}, which imply that their interrelation was not significant.


(a)

(b)
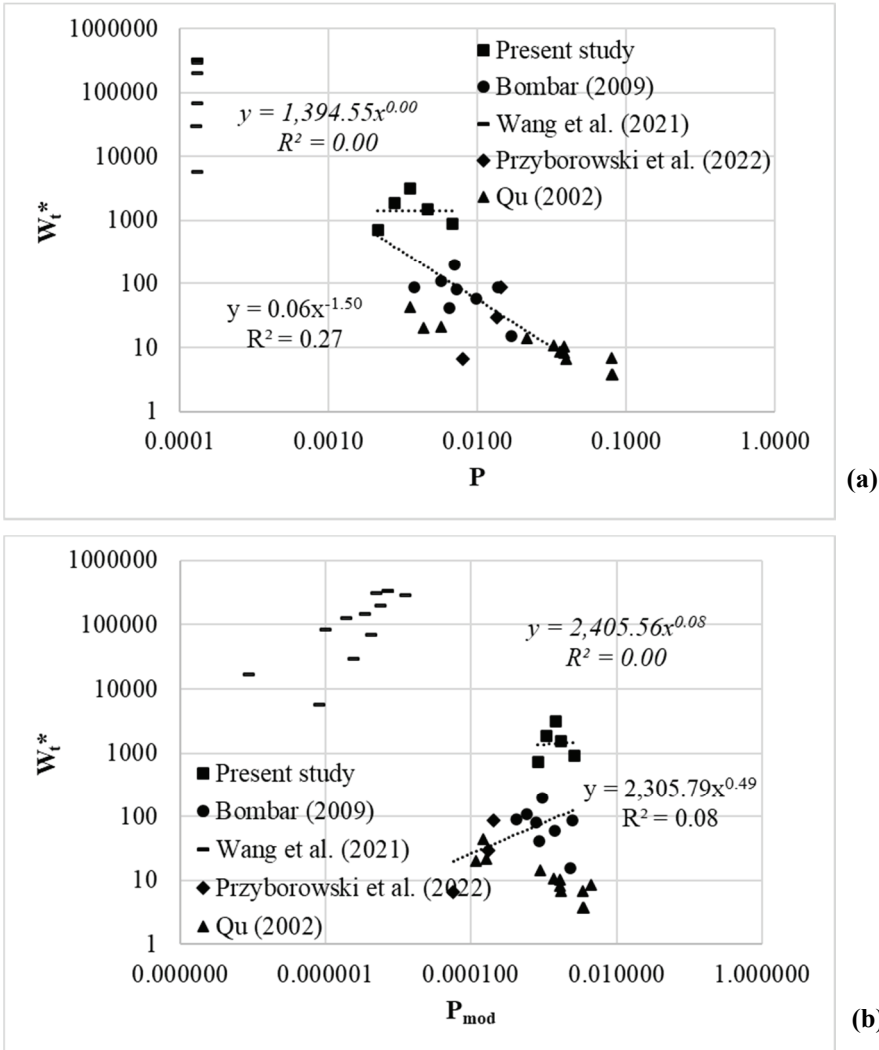
Figure 19 - Variation of dimensionless total bed load Wt* with the unsteadiness parameter (a) P, (b) P_{mod}

The variation of the dimensionless total bed load versus the unsteadiness parameter P_{gt} is plotted in Figure 20, together with the data of Bombar (2009), those of Qu (2002), Wang et al. (2021) and Przyborowski et al. (2022). Four experiments of Qu (2002) and the experiments of Wang et al. (2021) seem to deviate from the given exponential relation. The reason is proposed to be the difference between the range of time durations such that the tr

of Qu (2002) for those is 10 seconds and all experiments of Wang et al. (2021) is longer than 60 mins which is 12 times greater than those experiments focused in this study. Note that when the duration is sufficiently long the unsteadiness parameter P_{gt} has almost no affect on the W_t^*. Excluding these set of experiments, the high value of the determination coefficient of 0.69 stands for an appreciable interdependence. The SI values are 1.58, 2.24 and 2.17 for P_{gt}, P and P_{mod}, respectively.
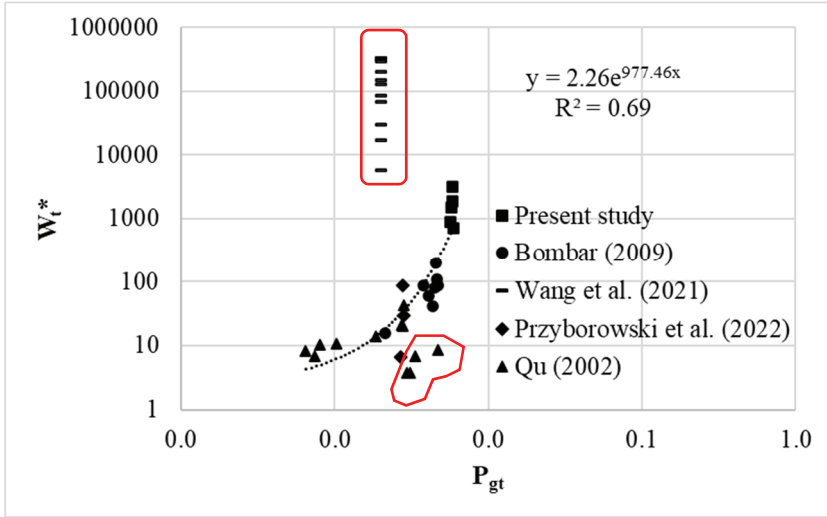

Figure 20 - Variation of unsteadiness parameter W_t^* with dimensionless total bed load P_{gt}

4. CONCLUSION

The aim of this experimental study is to investigate the unsteadiness effects on the transport of bimodal bed material. A clockwise behavior was observed in the total bed load - shear velocity curve which means that the bed load was higher on the rising limb compared to that of the falling limb.

From the variation of the grain size distribution with respect to time, it was found that the percent finer at the plateau of bimodal sediment size distribution curve had higher values during the initial and final phases compared to those obtained during the peak time. At all plateaus, the percent finer values related to the hydrograph peak discharge were in the same order of magnitude with that of the bed material.

It was observed that in all experiments the bimodality index B* increased quickly in the rising limb and then had a nearly constant value slightly greater than that of the bed material, eventually reaching its initial value.

The sand content of the transported bed material decreased rapidly $\cong$ from $\cong$ 96 % to $\cong$ 30% – 40% which was the original sand content of the bed material. The sand content remained constant for a while and gradually increased at the end of the hydrograph.

The variation of the percent sand content of the bed load with respect to the shear velocity revealed that the sand percent of the bed load decreased in the falling limb showing a counterclockwise loop and the duration of the hydrograph did not affect the results considerably, within the limits of the experimental campaign. On the other hand, the greater peak flow rate of the hydrograph resulted in greater hysteresis.

The values of D_5, D_{50} and D_{95} were determined from the cumulative grain size distribution curves of the collected sediments. The 5% finer sediment amount was nearly equal during rising and falling limbs. It was observed that D_{50} value of the bed load decreased in the rising limb showing a clockwise loop. The hysteresis was not considerably changed according to the hydrograph characteristics. The clockwise type hysteresis was also observed for the size group of D_{95}. The lag increased as the peak flow rate increased.

A strong relation was found between the dimensionless total bed load W_t^* and the total work index W_k with a determination coefficient $R^2 = 0.81$. The determination coefficient R^2 between W_R/W_F and W_k was found as 0.73.

The correlations between the dimensionless total bed load and the unsteadiness parameters P, and particularly for P_{mod} were very weak which imply that their interrelation was not significant. As to the unsteadiness parameter P_{gt}, the high value of determination coefficient of 0.69 stands for an appreciable interdependence. Considering the complexity of the unsteadiness parameter P_{mod}, it is revealed that within the limitations of this study which are given in Table 6, Pgt together with Wk could be used to calculate the Wt* for unsteady flows.

Table 6 - Limitations of the present study

Parameter	Minimum value	Maximum value
D_{50} (mm)	3.4	5.8
h_b (m)	0.02	0.12
h_p (m)	0.09	0.22
Q_b (l/s)	12.0	30.3
Q_p (l/s)	63.7	86.3
t_f (min)	0.2	5.0
t_r (min)	0.5	5.0
S_o (m/m)	0.002	0.006
P_{gt}	0.0038	0.0047
W_k	2.0	35.6
W_t^*	41	197

References

[1] Bombar, G., 2009, Experimental and numerical investigation of bed load transport in unsteady flows, October 2009, PhD Thesis, Dokuz Eylül University Graduate School of Natural And Applied Sciences.

[2] Bombar, G., Elçi, Ş., Tayfur, G., Güney, M.Ş., Bor, A., 2011, Experimental and numerical investigation of bedload transport under unsteady flows, Journal of Hydraulic Engineering. posted ahead of print February 25, 2011. doi:10.1061/(ASCE)HY.1943-7900.0000412

[3] De Sutter, R., Verhoeven, R., Krein, A., 2001, Simulation of sediment transport during flood events: laboratory work and field experiments. Hydrological Sciences-Journal-des Sciences Hydrologiques, 46(4), 599-610.

[4] Duan, Z., Chen, J., Jiang, C., Liu, X., and Zhao, B., 2020, Experimental Study on Uniform and Mixed Bed-Load Sediment Transport under Unsteady Flow Appl. Sci. 2020, 10, 2002; doi:10.3390/app10062002

[5] Gumgum, F., Guney, M.S., 2021, Effect of Sediment Feeding on Live-Bed Scour around Circular Bridge Piers, Civil Engineering Journal, Vol. 7, No. 05, pp 906-914, DOI:10.28991/cej-2021-03091699

[6] Güney, M.Ş., Bombar G.,Aksoy A.Ö., 2013, Experimental study of the coarse surface development effect on the bimodal bed load transport under unsteady flow conditions, Journal of Hydraulic Engineering, Vol. 13, No. 1, pp 12-21. DOI: 10.1061/(ASCE)HY.1943-7900.0000640.

[7] Gunsolus, E.H., Andrew, B.D., 2017, Effect of morphologic and hydraulic factors on hysteresis of sediment transport rates in alluvial streams River Res Applic. 2018;34:183–192. DOI: 10.1002/rra.3184

[8] Gunsolus, E.H., Binns, A.D. 2017, Effect of morphologic and hydraulic factors on hysteresis of sediment transport rates in alluvial streams, River Research and Applications, Vol. 34, No. 2, pp 183-192 . DOI:10.1002/rra.3184

[9] Houssais, M., Lajeunesse E., 2012, Bedload transport of a bimodal sediment bed, Journal of Geophysıcal Research, Vol. 117, F04015, DOI:10.1029/2012JF002490,

[10] Khosravi, K., Chegini, A.H.N., Binns, A.D., Daggupati, P. and Mao, L., 2019, Difference in the bed load transport of graded and uniform sediments during floods: An experimental investigation Hydrology Research | 50.6

[11] Kuhnle, R.A., 1992, Bed load transport during rising and falling stages on two small streams, Earth Surface Processes and Landforms, Vol 17, 191-197

[12] Lee, K.T., Liu, Y.L., Cheng, K.H. 2004, Experimental investigation of bedload transport processes under unsteady flow conditions, Hydrological processes, 18(13), pp. 2439-2454.

[13] Li, Z., Qian, H., Cao, Z., Liu, H., Pender, G., Hu, P., 2018, Enhanced bedload sediment transport by unsteady flows in a degrading channel International Journal of Sediment Research 33 327–339 https://doi.org/10.1016/j.ijsrc.2018.03.002

[14] Mao, L., 2012, The effect of hydrographs on bed load transport and bed sediment spatial arrangement, Journal of Geophysical Research Atmospheres, Vol. 117, F03024, DOI:10.1029/2012JF002428

[15] Mao, L., 2018, The effects of flood history on sediment transport in gravel-bed rivers Geomorphology 322 (2018) 196–205 https://doi.org/10.1016/j.geomorph.2018.08.046.

[16] Melville, B., Sutherland, A. 1988, Design method for local scour at bridge piers, Journal of Hydraulic Engineering, Vol. 114, No. 10, pp 1210–1226.

[17] Mrokowska, M.M. and Rowinski, P.M., 2019, Impact of Unsteady Flow Events on Bedload Transport: A Review of Laboratory Experiments Water 2019, 11, 907; doi:10.3390/w11050907

[18] Müller, E.N., Batalla R.J., Bronstert A., 2008, Modelling bedload transport rates during small floods in a gravel-bed river. Journal of Hydraulic Engineering 134, 1430-1439

[19] Nanson, G.C., 1974, Bedload and suspended load transport in a small, steep, mountain stream, Am. Journal Sci., 274, 471-486.

[20] Przyborowski L., Nones M., Mrokowska M., Książek L., Phan C.N., Strużyński A., Wyrębek M., Mitka B., Wojak S., 2022, Preliminary evidence on laboratory experiments to detect the impact of transient flow on bedload transport, Acta Geophysica, https://doi.org/10.1007/s11600-022-00743-5Parker G, 2008, "Chapter 3, Transport of Gravel and Sedıment Mıxtures", ASCE Manual 54, http://hydrolab.illinois.edu/people/parkerg/_private/Man54/Man54Chap3WholeText.pdf

[21] Parker's Morphodynamics Web Page, (2006a, Calculator for statistical characteristics of grain size distributions: http://hydrolab.illinois.edu/people/parkerg/_private/e-bookExcel/RTe-bookGSDCalculator.xls

[22] Parker's Morphodynamics Web Page, 2006b, Characterization of Sediment and Grain Size Distributions: http://hydrolab.illinois.edu/people/parkerg/_private/e-bookPowerPoint/RTe-bookCh2SedimentGSD.ppt

[23] Perret, E., Berni, C., Camenen, B., Herrero, A., Abderrezzak, K.E. 2018, Transport of moderately sorted gravel at low bed shear stresses: The role of fine sediment infiltration. Earth Surf. Process. Landforms, 43, 1416–1430.

[24] Plumb, B.D., Juez, C., Annable, W.K., McKie1, C.W., and Franca, M.J., 2020, The impact of hydrograph variability and frequency on sediment transport dynamics in a gravel-bed flume Earth Surf. Process. Landforms 45, 816–830 (2020) DOI: 10.1002/esp.4770

[25] Qu, Z., 2002, Unsteady open-channel flow over a mobile bed, PhD Thesis, EPFL, Thesis no 2688

[26] Reid, I., Frostick L.E., Layman J.T., 1985, The incidence and nature of bedload transport during flood flows in coarse-grained alluvial channels, Earth Surface Processes and Landforms, Vol 10, 33-44

[27] Saadi, Y., 2008, Fractional Critical Shear Stress at incipient motion in a bimodal sediment, Civil Engineering Dimension, Vol 10, No 2, pp 89-98

[28] Sambrook Smith G.H., 1996, Bimodal fluvial bed sediments: origin, spatial extent and processes, Progress in Physical Geography, Vol 20, No 4, pp 402-417, DOI: 10.1177/030913339602000402

[29] Smith Nicholas Ferguson, 1997, Measuring and defining bimodal sediments: Problems and implications, Water Resources Research, Vol 33, pp 1179-1185

[30] Tabarestani, M., Zarrati, K. 2015, Sediment transport during flood event: a review Int. J. Environ. Sci. Technol. 12:775–788 DOI 10.1007/s13762-014-0689-6

[31] Tian, S. and Wang Z., 2009, Bimodal sediment distribution and its relation with the river ecology in the Dadu River Basin, Advances in Water Resources and Hydraulic Engineering, pp 1049-1054

[32] Wang, L., Cuthbertson, A., Pender, G., 2013, Experimental investigation on temporal lag effect of graded sediment transport in unsteady flows Proceedings of 2013 IAHR Congress © 2013 Tsinghua University Press, Beijing

[33] Wang, L., Cuthbertson, A., Pender, G., Cao, Z., 2014, The Response of Bed-load Sediment Transport and Bed Evolution under Unsteady Hydrograph Flows, River Flow 2014 Conference: River Flow 2014 – the 7th International Conference on Fluvial Hydraulics At: Lausanne, Switzerland September 2014 DOI: 10.1201/b17133-215

[34] Wang, L., Cuthbertson, A., Pender, G., Cao, Z., 2015, Experimental investigations of graded sediment transport under unsteady flow hydrographs International JournalofSedimentResearch30(2015)306–320 http://dx.doi.org/10.1016/j.ijsrc.2015.03.010

[35] Wang, L., Wang, D., Cuthbertson, A.J.S., Zhong, D., and Pender, G., 2021a, Hysteretic Implications for Graded Bed Load Sediment Transport in Symmetrical Hydrograph Flows. Front. Environ. Sci. 9:800832. doi: 10.3389/fenvs.2021.800832

[36] Wang, L., Cuthbertson, A.J.S., Zhang, S.H., Pender, G., Shu, A.P., Wang, Y.Q., 2021b, Graded bed load transport in sediment supply limited channels under unsteady flow hydrographsWaters, K.A., and Curran, J.C., 2015, Linking bed morphology changes of two sediment mixtures to sediment transport predictions in unsteady flows, Water Resour. Res., 51, 2724–2741, doi:10.1002/2014WR016083.

[37] Wilcock, P.R., 1988, Methods for estimating the critical shear stress of individual fractions in mixed-size sediment, Water Resources Research, Vol 24, No 7, pp 1127 – 1135

[38] Wilcock, P.R., 1993, Critical shear stress of natural sediments, Journal of Hydraulic Engineering, Vol 119, No 4, April, pp 491 – 505

[39] Wilcock, P.R., Kenworthy S.T., Crowe J., 2001, Experimental study of the transport of mixed sand and gravel, Water Resources Research, Vol 37, No 12, pp: 3349-3358

[40] Wilcock, P.R., 2001, Toward a practical method for estimating sedimenttransport rates in gravel-bed rivers, Earth Surf. Processes Landforms, 26(13), 1395–1408, doi:10.1002/esp.301.

[41] Wilcock, P.R., and Kenworthy S., 2002, A two-fraction model for the transport of sand/gravel mixtures, Water Resour. Res., 38(10), 1194, doi:10.1029/2001WR000684.

[42] Yarnell, S.M., Yager, E., Sasha, L., 2016, Impacts of Hydrograph Shape on Sediment Transport in a Gravel-Bedded Stream, Extended Abstract 11th ISE 2016, Melbourne, Australia